State-Selective Production of Vibrationally Excited NO_2^+ by Double-Resonant Photoionization†

Patrice Bell,‡,§ F. Aguirre,‡ E. R. Grant,§ and S. T. Pratt*,‡

Argonne National Laboratory, 9700 South Cass Avenue, Argonne, Illinois 60439, and Department of Chemistry, Purdue University, West Lafayette, Indiana 47907

Received: January 20, 2004; In Final Form: April 5, 2004

Two-color, two-photon resonant, three-photon ionization, and high-resolution photoelectron spectroscopy are combined to characterize the photoionization dynamics of the $3p\sigma\ ^2\Sigma_u^+$ electronic state of NO_2. Direct photoionization of selected vibrational levels of the NO_2 $3p\sigma\ ^2\Sigma_u^+$ state shows a strong propensity to preserve the vibrational quantum numbers of the intermediate state. Efficient methods for producing NO_2^+ X $^1\Sigma_u^+$ (000), (010), (100), and (001) with over 95% purity are discussed. This approach is expected to be applicable to the study of the mode dependence of the effects of vibrational excitation in ion−molecule reactions involving NO_2^+.

I. Introduction

The experimental conditions for ion−molecule reactions naturally afford opportunities to investigate collision-energy thresholds for chemical transformations.[1−5] The degree to which internal energy drives such reactions can provide additional dynamical insights, and with the advent of coincident photoelectron spectroscopy and PEPICO techniques introduced by Baer and co-workers,[6] it has become possible to compare cross sections for ions in different, well-defined initial vibrational states. Such photoelectron−photoion coincidence methodologies have been refined to the rotational level for some reactions by introduction of pulsed-field-ionization threshold photoelectron spectroscopic monitoring.[7,8]

Alternative approaches have tuned multiple-photon laser ionization pathways through specific intermediate resonances to actively produce populations of cations in selected vibrational states.[9−11] Studies using this direct strategy have successfully exposed reaction dynamics influenced not only by the total energy and its partitioning between translation and vibration but also by the topology of internal motion as determined by the combination of normal modes excited.[12,13] Such experiments rely on Franck−Condon factors that preserve vibrational quantum numbers in photoionization from selected intermediate Rydberg states.[14] In the present work, we show how this effect can be used along with the broad Franck−Condon envelope normally associated with the geometry changes typically encountered upon ionization of open-shell neutral molecules to allow the production of state-selected ions in a wide range of vibrational levels. Our molecule, NO_2, is representative of the important class of free radicals that transform from open-shell neutrals to yield closed-shell cations. We demonstrate by multiresonant photoelectron spectroscopy that efficient pathways exist for creating abundant populations of NO_2^+ ground state ions in the (000), (100), (010), and (001) vibrational levels with >95% purity.

The ion−molecule reactions of NO_2^+ are important in a number of contexts, including stratospheric chemistry involving protonated nitric acid,[15] high-temperature combustion,[16,17] and astrochemistry.[18] Studies of the vibrational mode dependence of the reactions of NO_2^+ are expected to be particularly informative. Unfortunately, conventional one-color multiphoton ionization has not provided an effective method for producing state-selected NO_2^+. This situation is a result of two effects. First, the geometry of ground state NO_2 is bent, while the ground state ion and the Rydberg states converging to it are linear. Thus, the Franck−Condon factors from the ground state to any of the low-lying vibrational levels of the Rydberg states are very small (with the exception of those involving the bending vibration), and this results in a very low efficiency for ion production. Second, when two-photon excitation is used to populate the Rydberg state, the energy of the first photon lies in a strong absorption band that leads to the dissociation of NO_2, which further reduces the efficiency of ion production. In addition, NO produced by this dissociation is efficiently ionized, leading to a large background of NO^+. Although this background can be removed by mass selecting the ions, it can still be a nuisance.

Our approach uses two-color, two-photon excitation to prepare selected vibrational levels of the $3p\sigma\ ^2\Sigma_u^+$ Rydberg state of NO_2, which are then photoionized by a single photon of either color. As shown by Grant and co-workers, this photoexcitation strategy exploits the vibronically mixed character of the states that form the visible absorption system of NO_2 to bridge the Franck−Condon gap between the bent neutral and the linear Rydberg state.[19−26] In the present paper, we combine this two-color approach with high-resolution photoelectron spectroscopy to characterize the direct photoionization dynamics of the $3p\sigma\ ^2\Sigma_u^+$ state. This work demonstrates that the two-color stepwise excitation can overcome the difficulties associated with one-color multiphoton ionization and be used to produce vibrationally state-selected NO_2^+ in all three normal modes. The results also provide insight into the photoionization dynamics of the $3p\sigma\ ^2\Sigma_u^+$ state.

II. Experimental Section

The experiments employ a magnetic bottle electron spectrometer to measure the velocities of electrons produced by

† Part of the special issue "Tomas Baer Festschrift".
‡ Argonne National Laboratory.
§ Purdue University.

10.1021/jp0400364 CCC: $27.50
Published on Web 05/19/2004

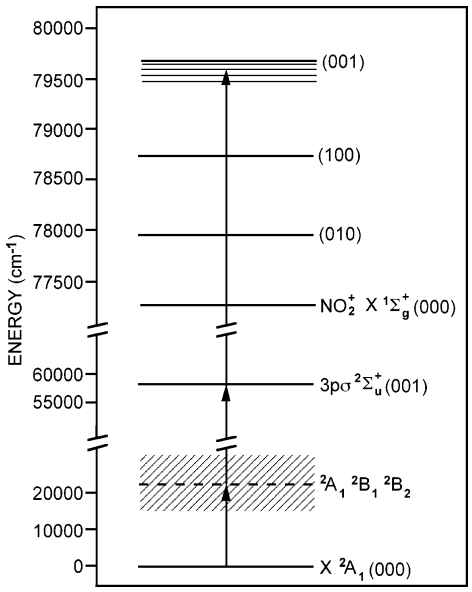

Figure 1. Schematic energy level diagram showing the relevant energy levels of NO_2. The first photon, λ_1, accesses a selected level within a region of high vibronic state density associated with levels of the $^2B_1$, $^2B_2$, and $^2A_2$ excited states, all of which are vibronically coupled with X $^2A_1$. The second laser, λ_2, drives the transition from this selected level to a selected rotational level of the 3pσ Σ_u^+ (001) Rydberg state (for example). Ionization occurs by absorption of a photon at either λ_1 or λ_2.

TABLE 1: Ionization Thresholds for Relevant Vibronic Levels of NO_2^+ $X^1\Sigma_g^+$

vibronic state	ionization threshold (cm^{-1})
(000)	77316.7[a]
(010)	77943.6[a]
($02^{\circ}0$)	78551.1[a]
(02^20)	78559.4[a]
(100)	78703.5[b]
(03^10)	79186.8[c]
(03^30)	79212.8[c]
(001)	79678.7[a]

[a] Values are taken from ZEKE experiments (ref 22) and the ionic vibrational levels (ref 26). [b] Value is taken from ZEKE experiments (ref 22). [c] Values are taken from ZEKE (ref 22) and the 3pσ Rydberg Q-branch assignments (ref 23).

stepwise photoionization using two nanosecond pulsed Nd:YAG-pumped dye lasers. As shown in Figure 1, the selected vibrational level of the 3pσ $^2\Sigma_u^+$ state is populated by a two-photon transition involving one photon of λ_1 and one of λ_2. Here, λ_1 corresponds to the fundamental output of the first laser, while λ_2 corresponds to the frequency-doubled output of the second laser. The pulse energies of λ_1 and λ_2 are approximately 5 mJ and 0.5 mJ, and the bandwidths are 0.03 and 0.1 cm^{-1}, respectively. The values of λ_1 and λ_2 are chosen so that a single photon of λ_1 cannot dissociate the NO_2 but could still ionize the selected intermediate level via a vertical transition (i.e., without a change in the vibrational quantum numbers of the intermediate state). The first photon at λ_1 excites the NO_2 to a region of very high density of states produced by the complex vibronic structure of three interacting electronic states. The pulses of the two lasers overlap in time, and because λ_2 is considerably shorter than λ_1, the intermediate state can be ionized by the absorption of one photon from either laser. The relevant ionization thresholds are given in Table 1.

The two laser beams copropagate collinearly, and focus loosely into the collision zone of the electron spectrometer, where they cross the molecular beam of NO_2. The molecular beam is produced by expanding a 1:1:20 mixture of NO_2/O_2/He at a stagnation pressure of 1000−1500 Torr into a vacuum chamber by using a piezoelectric pulsed valve. The resulting beam is skimmed approximately 5 cm downstream of the nozzle and crossed perpendicular to the laser beams in the interaction region. The wavelengths of the two lasers were optimized by performing scans of λ_1 with λ_2 fixed, and of λ_2 with λ_1 fixed, while monitoring the total photoelectron yield. In addition, lock scans were performed by scanning λ_1 up and λ_2 down while maintaining a constant photon energy. This process was repeated for the 3pσ $^2\Sigma_u^+$ (000), (100), (010), and (001) intermediate states, where the labeling (υ_1,υ_2,υ_3) corresponds to the symmetric stretch, υ_1, the bend, υ_2, and the asymmetric stretch, υ_3, respectively. Optimizing λ_1 can result in improved Franck−Condon factors for the overall two-photon transition to the selected vibrational level of the 3pσ $^2\Sigma_u^+$ state, and greatly enhance the ionization yield. While the high density of states at the one-photon energy ensures that a resonance will be nearby, as discussed below, it also can make it difficult to assign the structure in the two-photon spectrum. The lasers were calibrated by using the optogalvanic effect in Ar, Ne, and U, and by using commercial wavemeters.

The magnetic bottle electron spectrometer has been described previously.[27−29] Briefly, the photoelectrons are produced in a region of 1-T magnetic field, which diverges from 1 to 10^{-3} T at the entrance to the flight tube. The diverging field acts to parallelize the trajectories of the photoelectrons, while maintaining information on their velocities. Thus, high-resolution photoelectron spectra can be recorded with high collection efficiency. The drift tube can be biased to provide a retarding or accelerating potential. The resolution for the present experiment is ∼7 meV for electrons with energies less than 0.1 eV and considerably lower for the fast photoelectrons produced by the ($\lambda_1 + \lambda_2 + \lambda_2$) process. Nevertheless, this resolution is sufficient to resolve the vibrational structure of interest. The rotational constant of NO_2^+ is too small to allow the observation of resolved rotational structure in the photoion.

The photoelectron time-of-flight traces for individual laser shots are recorded by sending the signal from a dual channelplate detector to a digital oscilloscope. Typically, data from 3000 laser shots are averaged to produce a photoelectron spectrum. The low photoelectron energies resulting from the ($\lambda_1 + \lambda_2 + \lambda_1$) process makes it necessary to apply a potential of approximately −0.4 V to a grid in the interaction region to push the electrons into the flight tube of the spectrometer. To obtain reasonable resolution for the fast photoelectron peaks produced by the ($\lambda_1 + \lambda_2 + \lambda_2$) process, we recorded separate photoelectron spectra with a retarding voltage applied to the flight tube grid. As discussed previously,[24,25] photoelectron spectra were calibrated by using the energies of photoelectron peaks corresponding to known photoionization processes. In particular, the vertical photoelectron peaks resulting from ($\lambda_1 + \lambda_2 + \lambda_1$) and ($\lambda_1 + \lambda_2 + \lambda_2$) photoionization above the X $^1\Sigma_g^+$ ($\upsilon_1\upsilon_2\upsilon_3$) thresholds were used, as well as the NO^+ (X $^1\Sigma^+$, $\upsilon^+ = 0$) photoelectrons produced by λ_1 ionization of NO (A $^2\Sigma^+$) state. Calibration uncertainty was ±5 meV for the low-energy photoelectrons.

III. Spectroscopic Considerations

The symmetry labels and selection rules relevant to the present experiment have been discussed in detail previously.[25,26,30] In what follows, the quantum numbers of the ground state are labeled with double primes, those of the 3pσ $^2\Sigma_u^+$ intermediate state with single primes, and those of the ion with

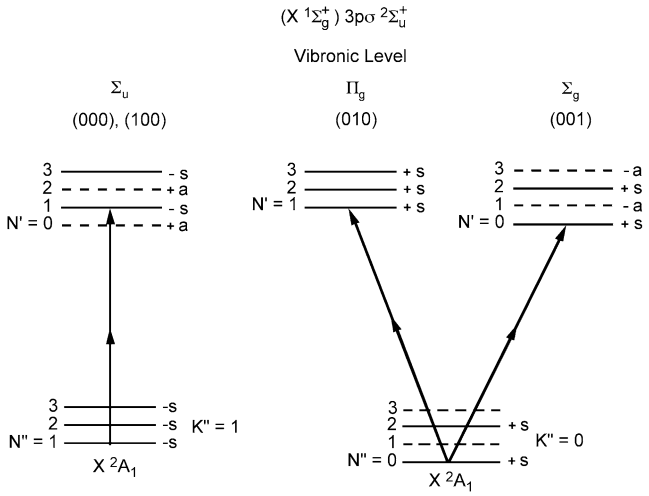

Figure 2. Rotational level diagram indicating rovibrational symmetries in the 3pσ Rydberg state and two-photon transitions allowed from the X $^2A_1$ ground state.

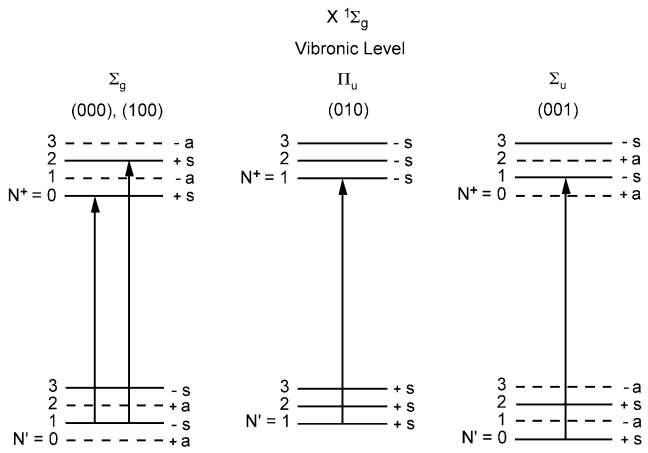

Figure 3. Rotational level diagram indicating rovibrational symmetries in the X $^1\Sigma_g^+$ cation ground state and two-photon transitions allowed from the 3pσ Σ_u^+ intermediate state.

plus signs. As in earlier work,[25,26] the selection rules for the X $^2A_1$ to 3pσ $^2\Sigma_u^+$ transition will be considered in terms of the overall two-photon transition. The two most important symmetry elements common to the NO_2 X $^2A_1$ ground state, the 3pσ $^2\Sigma_u^+$ intermediate state, and the electron−ion complex are the inversion symmetry (or total parity), ±, and the permutation symmetry for exchange of the oxygen nuclei, s/a. Because the terminal ^{16}O nuclei are spin-zero bosons, the permutation symmetry of all of the levels that exist must be s. The $K'' = 0$ levels of the X $^2A_1$ vibrational ground state have + symmetry, and, as shown in Figure 2, only those with N'' = even, which have (+,s) symmetry, exist. For $K'' = 1$, all allowed levels have (−,s) symmetry.

Figure 2 also shows symmetry assignments for the first few rotational levels for the Σ_u, Π_g, Σ_g vibronic levels of the 3pσ $^2\Sigma_u^+$ Rydberg state. As a result of the different u and g symmetries for the different vibronic levels, accessing the desired 3pσ $^2\Sigma_u^+$ vibronic level requires starting from a suitable K'' level. In the Π_g vibronic components [e.g., (010)], only the levels with (+,s) symmetry and $N' \geq 1$ exist. In the Σ_u vibronic states [e.g., (000), (100)], one finds only levels with (−,s) symmetry and N' = odd, while the Σ_g vibronic states [e.g., (001)] support only those levels with (+,s) symmetry and N' = even. The permutation symmetry is set by nuclear spin statistics, and the selection rules for the two-photon transition between the X $^2A_1$ ground state and the 3pσ $^2\Sigma_u^+$ Rydberg state require that the inversion symmetry does not change (+ → +, − → −). Thus, transitions to states of vibronic symmetry Π_g or Σ_g [(010) or (001), respectively] can only originate from K'' = even levels, 0, 2, ..., and transitions to Σ_u levels [i.e., (000), (100)] can only originate from $K'' = 1$ levels (or more generally, from K'' = odd levels).

As discussed by Bryant et al.,[21,22] the selection rules for a single-photon transition from the 3pσ $^2\Sigma_u^+$ state to the ionization continuum constrain the inversion symmetry and permutation symmetry transformations to + → −, and s → s, respectively. The 3pσ $^2\Sigma_u^+$ state and the NO_2^+ X$^1\Sigma_g^+$ state are both linear, so there is also a u → g selection rule on the vibronic symmetry. As in the 3pσ $^2\Sigma_u^+$ state, nuclear spin statistics restrict the rotational levels of the NO_2^+ X $^1\Sigma_g^+$ ion that can exist. These restrictions are shown in Figure 3. In particular, the Π_u vibronic levels have (−,s) symmetry, and levels exist for all $N^+ \geq 1$. The Σ_g vibronic levels have (+,s) symmetry, and levels exist for all N^+ = even. The Σ_u vibronic levels have (−,s) symmetry, and levels exist for all N^+ = odd.

IV. Results and Discussion

IV.A. Ionization-Detected Absorption Spectra. The preparation of selected vibrational levels of the 3pσ $^2\Sigma_u^+$ state of NO_2 relies heavily on the previous studies of the spectroscopy of this state by Grant and co-workers.[19−24] The vibrational levels of interest are fairly well separated from neighboring levels so that it is not difficult to select the vibronic level of interest by a suitable choice of λ_1 and λ_2. However, the detailed assignment of the rotational level in the selected vibronic level of the 3pσ $^2\Sigma_u^+$ state is considerably more challenging. In principle, once a two-photon resonance is found, one could scan λ_1 with λ_2 fixed, or scan λ_2 with λ_1 fixed on a particular pump transition. In the former case, the λ_1 spectrum would show peaks corresponding to transitions from several rotational levels in the X $^2A_1$ state to the selected lower rotational level of the λ_2 transition. This approach has worked quite well in some studies by Grant and co-workers.[19−24] Unfortunately, perhaps due to the considerably shorter wavelength of λ_1 in the present experiments, the density of states at the energy of λ_1 appears to be high enough that λ_2 is resonant with more than one rovibronic transition. This high density of optically accessible states results from complex vibronic interactions among three different excited electronic states of NO_2. This situation makes it difficult to assign the N'' value of the two-photon transition. Similarly, if λ_1 is fixed and λ_2 is scanned, a small number of peaks corresponding to transitions from the selected intermediate level to the allowed rotational levels ($\Delta J = 0, \pm 1$) in the 3pσ $^2\Sigma_u^+$ state should be observed. This spectrum should then support an assignment of the N' value in the 3pσ $^2\Sigma_u^+$ state. Again, as a result of the high density of states at the one-photon energy, λ_1 does not appear to pump a single rovibronic transition, and the resulting λ_2 spectrum typically contains many more than three lines. The wavelengths used to excite the different vibronic levels are given in Table 2. The most likely rotational assignments for the two-photon transitions used in the present study are provided in Table 3, but these should be regarded as provisional.

An additional factor that contributes to the complexity of the two-photon spectra is the presence of the 1-T magnetic field in the interaction region. Although this field is necessary to achieve high collection efficiency for the photoelectron spectra, it is

TABLE 2: Excitation Wavelengths for the NO_2^+ Vibrational Levels Studied

v_1', v_2', v_3'	λ_1 (nm)[a]	λ_2 (nm)[a]
(000)	455.598	296.900
(010)	455.737	291.407
(100)	456.000	284.901
(001)	459.699	276.054

[a] The error bars for the wavelengths are ±0.001 nm.

TABLE 3: Tentative Rotational Assignments for the Two-Photon Transitions

$3p\sigma\ ^2\Sigma_u^+$ v_1', v_2', v_3'	N''	N'	energy (cm^{-1}) [v_1]	energy (cm^{-1}) [v_2]
(000)	1	5	21949.2	33681.4
(010)	0	3	21942.5	34316.3
(100)	1	5	21929.8	35100.0
(001)	2	4	21753.4	36224.9

possible to record wavelength scans of both λ_1 and λ_2 with the electromagnet turned off, albeit with a poorer signal-to-noise ratio. Comparison of such "field-off" spectra with "field-on" spectra shows that the latter are considerably more complex, with many lines showing splittings and a significant number of extra lines. While the Zeeman effect in the ground state of NO_2 is well-characterized,[31] it is considerably less characterized at the one-photon energy,[32] and is a subject of active research.[33] In contrast, the Zeeman effect in the $3p\sigma\ ^2\Sigma_u^+$ state is likely relatively simple, as the state appears to be relatively isolated. In that case, the Rydberg electron is expected to act more or less as a free electron, with a splitting of approximately $2\mu_B B$ between the $M_S = \pm 1/2$ levels of a given state, where μ_B is the Bohr magneton of ~0.467 cm^{-1}/T and B is the field in tesla.[34] This splitting can be observed in the double-resonance spectra via the $3p\sigma\ ^2\Sigma_u^+$ state. Levels with different values of M_N will also be split by the field, but these splittings are not expected to be resolved at the present field strength and laser resolution. Although weak field-induced mixing with other states may occur, and although the magnetic field increases the complexity of the two-photon transition to the $3p\sigma\ ^2\Sigma_u^+$ state, the photoelectron spectra reported below suggest that the vibronic character of the selected levels are not substantially modified by the field.

Before moving to the photoelectron spectra, it is worth discussing the enhancement of the two-photon $3p\sigma\ ^2\Sigma_u^+ \leftarrow X\ ^2A_1$ transition that is achieved by using a two-color excitation process. As discussed above, the first benefit results from choosing a λ_1 photon energy that is below the dissociation threshold for NO_2. A second benefit is that the two-color process allows both steps to be resonant, leading to a significant enhancement over a nonresonant two-photon transition. Finally, although it is difficult to characterize, it is possible that the optimization of λ_1 and λ_2 can significantly improve the overall Franck−Condon factor between the bent $X\ ^2A_1$ state and the linear $3p\sigma\ ^2\Sigma_u^+$ state. This can be understood as follows. If the geometry and potential surface of the intermediate state is identical to that of the ground state, the Franck−Condon factor for the λ_1 transition will be unity, but the Franck−Condon factor for the λ_2 transition (and thus the product of Franck−Condon factors for the overall transition) will be the same as that for the one-photon $3p\sigma\ ^2\Sigma_u^+ \leftarrow X\ ^2A_1$ transition. Similarly, if the intermediate state is identical to the $3p\sigma\ ^2\Sigma_u^+$ state, the Franck−Condon factor for the λ_2 transition will be unity, but that for the λ_1 transition will be the same as that for the one-photon $3p\sigma\ ^2\Sigma_u^+ \leftarrow X\ ^2A_1$ transition. In either case, the overall Franck−Condon factor will be very small. However, if the intermediate state has a geometry intermediate between that of the $X\ ^2A_1$ and $3p\sigma\ ^2\Sigma_u^+$ states (or an indeterminate geometry owing to vibronic coupling), it is possible that the Franck−Condon factors for both the λ_1 and λ_2 transitions will be significant, with the overall product Franck−Condon factor being substantially larger than that for the one-photon $3p\sigma\ ^2\Sigma_u^+ \leftarrow X\ ^2A_1$ transition. While the spectroscopy at the first-photon energy is incredibly complex and unassigned, the lock-scan method allows an empirical approach for optimizing the Franck−Condon overlaps, as well as the electronic transition moments, for the two-photon transition.

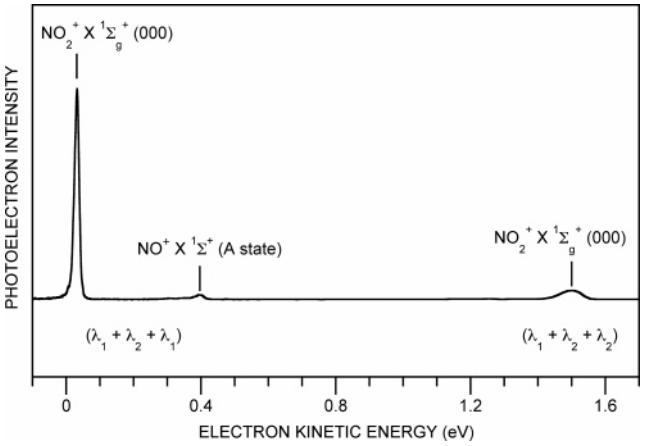

Figure 4. Photoelectron spectrum following direct ionization via the $3p\sigma\ ^2\Sigma_u^+$ (000) level with a small retarding voltage on the flight tube. The weak peak labeled $NO^+\ X\ ^1\Sigma^+$ (A state) is assigned to the one-photon λ_2 ionization of NO A $^2\Sigma^+$ produced by the multiphoton dissociation of NO_2.

IV.B. Photoelectron Spectra. The photoelectron spectrum for the $3p\sigma\ ^2\Sigma_u^+$ (000) band recorded with a minimal retarding voltage on the flight tube is shown in Figure 4. The low-energy (<0.5 eV) peaks in this spectrum are well resolved, but the faster peak near 1.5 eV is not resolved. The slowest peak corresponds to the ionization of the $3p\sigma\ ^2\Sigma_u^+$ (000) level by one photon at λ_1, that is, by a $(\lambda_1 + \lambda_2 + \lambda_1)$ process. The fastest peak is produced by ionization of the $3p\sigma\ ^2\Sigma_u^+$ (000) level by one photon at λ_2, that is, by a $(\lambda_1 + \lambda_2 + \lambda_2)$ process. As a result of the nature of the time-of-flight spectrometer, the instrumental width of the peaks broaden with decreasing flight time. The widths of the higher energy peaks can be reduced by applying a retarding voltage to increase the flight times. Figure 5 shows a portion of a second spectrum via the same intermediate level that was recorded with a larger retarding voltage on the flight tube. This provides significantly better resolution for the faster photoelectron peaks. The spectrum in Figure 4 also shows a photoelectron peak resulting from the ionization of NO in the A $^2\Sigma^+$ state. NO is present as an impurity in the gas cylinder and is also produced by the multiphoton dissociation of NO_2, which may populate the A $^2\Sigma^+$ state; once identified, this NO peak is helpful in calibrating the photoelectron spectra. A weak peak in Figure 5 is also tentatively assigned to the $(\lambda_1 + \lambda_2 + \lambda_2)$ ionization of ground state NO $X\ ^2\Pi$. Because the photon energy at λ_1 is just barely above the $NO_2^+\ X^1\Sigma_g^+$ (000) ionization threshold, only a single slow photoelectron peak from NO_2 is observed in Figure 4. In contrast, the photon energy at λ_2 lies approximately 1.5 eV above the $NO_2^+\ X^1\Sigma_g^+$ (000) threshold, and there is the potential for producing $NO_2^+\ X^1\Sigma_g^+$ in a number of different vibrational levels. The dominance of the $NO_2^+\ X^1\Sigma_g^+$ (000) photoelectron peak in Figure 5 clearly

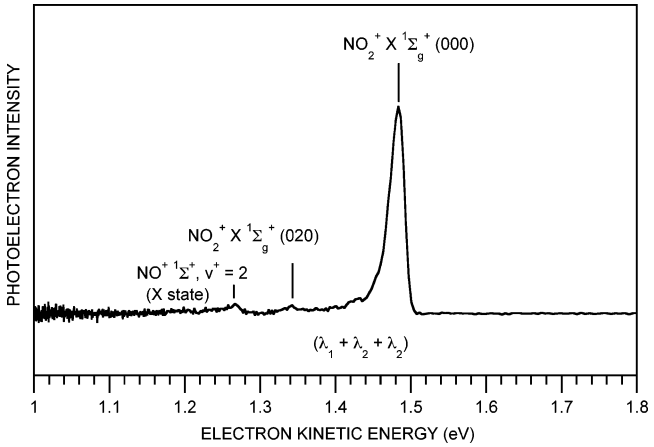

Figure 5. Photoelectron spectrum following direct ionization of the $3p\sigma\ ^2\Sigma_u^+$ (000) level. The spectrum was recorded with a retarding voltage on the flight tube to enhance the resolution of the $(\lambda_1 + \lambda_2 + \lambda_2)$ photoelectron peaks. The weak peak labeled NO^+ X $^1\Sigma^+$ (X state) is tentatively assigned to the photoionization of NO X $^2\Pi$ via a $(\lambda_1 + \lambda_2 + \lambda_2)$ process.

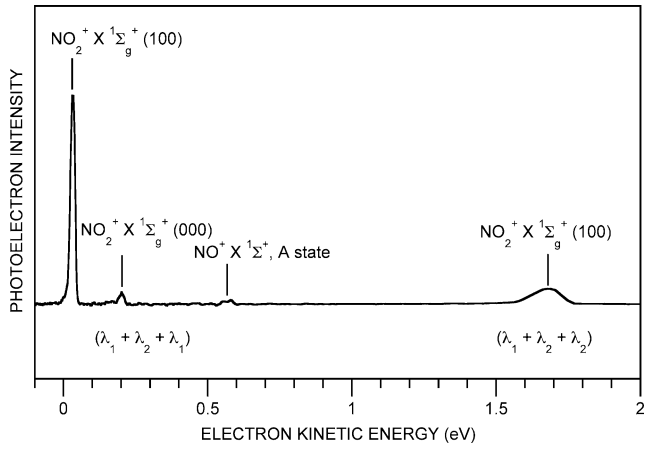

Figure 6. Photoelectron spectrum following direct ionization via the $3p\sigma\ ^2\Sigma_u^+$ (100) level with a small retarding voltage on the flight tube. The weak peak labeled NO^+ X $^1\Sigma^+$ (A state) is assigned to the one-photon λ_2 ionization of NO A $^2\Sigma^+$ produced by the multiphoton dissociation of NO_2.

indicates that the geometries and potential surfaces of the NO_2 $3p\sigma\ ^2\Sigma_u^+$ and NO_2^+ $X^1\Sigma_g^+$ states are very similar.

Pairs of photoelectron spectra for the NO_2 $3p\sigma\ ^2\Sigma_u^+$ (100), (010), and (001) bands are shown in Figures 6−11, respectively. These spectra are similar to those for the $3p\sigma\ ^2\Sigma_u^+$ (000) band, in that they show slow photoelectrons produced by the $(\lambda_1 + \lambda_2 + \lambda_1)$ process and fast photoelectrons produced by the $(\lambda_1 + \lambda_2 + \lambda_2)$ process. As in the (000) spectrum, the observed vibrational progressions for the $(\lambda_1 + \lambda_2 + \lambda_1)$ process are limited by the λ_1 photon energy and are all very short, while those for the $(\lambda_1 + \lambda_2 + \lambda_2)$ process are generally somewhat longer. Nevertheless, the vertical transitions (that is, where $v_1' = v_1^+, v_2' = v_2^+$, and $v_3' = v_3^+$) in both the $(\lambda_1 + \lambda_2 + \lambda_1)$ and $(\lambda_1 + \lambda_2 + \lambda_2)$ processes totally dominate the photoionization of the $3p\sigma\ ^2\Sigma_u^+$ state. The photoelectron branching fractions for the four intermediate vibrational levels and both the $(\lambda_1 + \lambda_2 + \lambda_1)$ and $(\lambda_1 + \lambda_2 + \lambda_2)$ ionization schemes are given in Table 4. Before discussing these branching fractions in more detail, the relative intensities of the $(\lambda_1 + \lambda_2 + \lambda_1)$ and $(\lambda_1 + \lambda_2 + \lambda_2)$ bands are first considered.

The relative intensities of the $(\lambda_1 + \lambda_2 + \lambda_1)$ and $(\lambda_1 + \lambda_2 + \lambda_2)$ processes in Figures 4, 6, 8, and 10 are determined by several

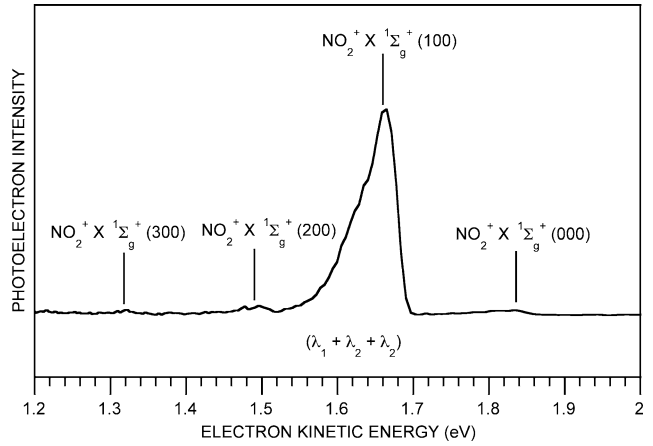

Figure 7. Photoelectron spectrum following direct ionization of the $3p\sigma\ ^2\Sigma_u^+$ (100) level. The spectrum was recorded with a retarding voltage on the flight tube to enhance the resolution of the $(\lambda_1 + \lambda_2 + \lambda_2)$ photoelectron peaks.

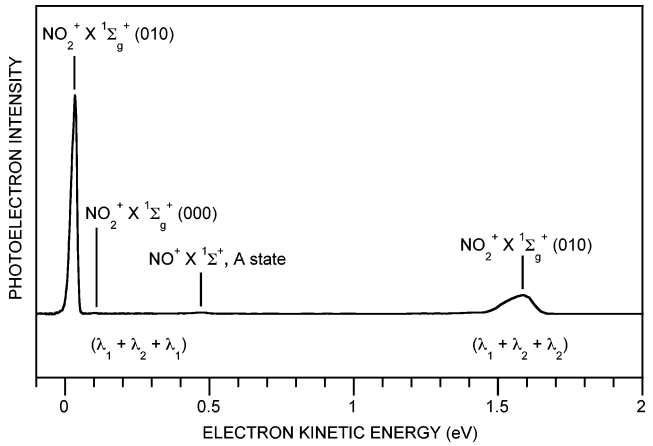

Figure 8. Photoelectron spectrum following direct ionization via the $3p\sigma\ ^2\Sigma_u^+$ (010) level with a small retarding voltage on the flight tube. The weak peak labeled NO^+ X $^1\Sigma^+$ (A state) is assigned to the one-photon λ_2 ionization of NO A $^2\Sigma^+$ produced by the multiphoton dissociation of NO_2.

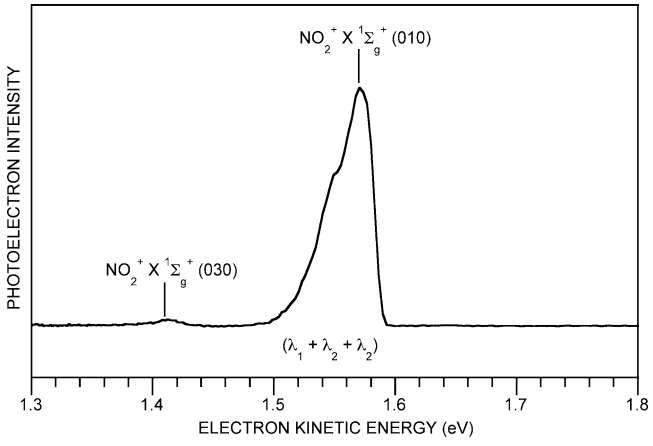

Figure 9. Photoelectron spectrum following direct ionization of the $3p\sigma\ ^2\Sigma_u^+$ (010) level. The spectrum was recorded with a retarding voltage on the flight tube to enhance the resolution of the $(\lambda_1 + \lambda_2 + \lambda_2)$ photoelectron peaks.

factors. The first is the relative intensity of the two laser beams, which was different in all four spectra. Although the pulse energy of the λ_1 beam is considerably larger than that of the λ_2 beam, the relative intensity in the interaction region is difficult to quantify. In particular, the beams were only loosely focused

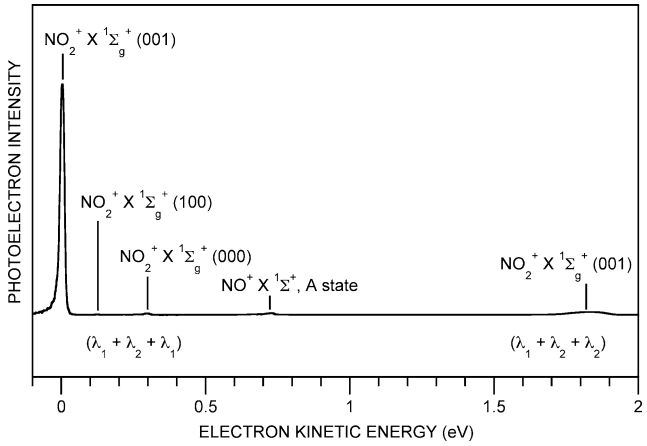

Figure 10. Photoelectron spectrum following direct ionization via the 3pσ $^2\Sigma_u^+$ (001) level with a small retarding voltage on the flight tube. The weak peak labeled NO^+ X $^1\Sigma^+$ (A state) is assigned to the one-photon λ_2 ionization of NO A $^2\Sigma^+$ produced by the multiphoton dissociation of NO_2.

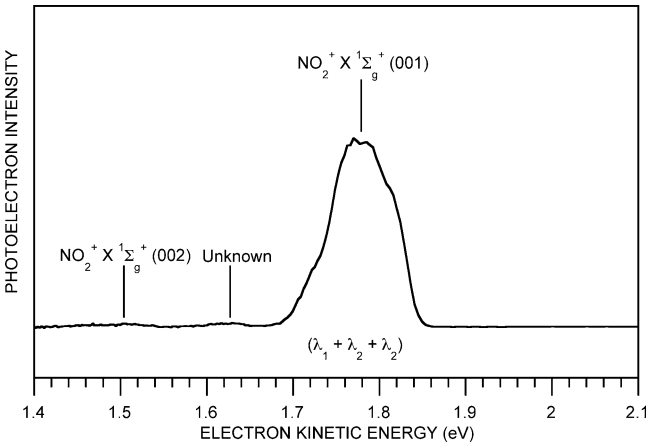

Figure 11. Photoelectron spectrum following direct ionization of the 3pσ $^2\Sigma_u^+$ (001) level. The spectrum was recorded with a retarding voltage on the flight tube to enhance the resolution of the ($\lambda_1 + \lambda_2 + \lambda_2$) photoelectron peaks.

into the interaction region and a nonachromatic lens was used, making it difficult to characterize the relative spot size of the two beams. The relative intensities of the two beams could be varied by introducing neutral density filters into the beam paths, and as expected, decreasing the intensity of a beam results in a decrease in the relative intensity of the corresponding photoelectron peaks. Even if the two beams had identical intensities in the interaction region, the ($\lambda_1 + \lambda_2 + \lambda_1$) process is expected to dominate because the electronic part of the photoionization matrix element for Rydberg states is typically greatest close to threshold and decreases substantially as the photon energy is increased well above the ionization threshold of the state.[35]

The observation that two different ionization processes [i.e., ($\lambda_1 + \lambda_2 + \lambda_1$) and ($\lambda_1 + \lambda_2 + \lambda_2$)] contribute to the photoelectron spectra of the 3pσ $^2\Sigma_u^+$ vibrational levels would create a problem in using this approach for producing state-selected ions if the vibrational branching fractions were significantly different for the two processes. Fortunately, Table 4 indicates that the ionization process creates state-selected ions with $\geq$96% purity regardless of the ionization path for all four 3pσ $^2\Sigma_u^+$ vibrational levels. Thus, control over which laser ionizes the intermediate state is not so important, and the relative intensities of the two can be optimized based on other considerations.

The observation that the vertical transition completely dominates the photoionization dynamics for the four vibrational levels of the 3pσ $^2\Sigma_u^+$ state studied clearly indicates that the potential surfaces for this state and the NO_2^+ $X^1\Sigma_g^+$ state are very similar, at least near the bottoms of their wells. The small signal observed for off-diagonal transitions could be readily explained in terms of small differences in the two surfaces, but their low intensity makes these difficult to quantify as several factors could influence the branching ratios. For example, the electronic photoionization matrix elements may depend on the electron kinetic energy and thus depend on the final vibrational level that is accessed. This effect would skew the distributions expected from the purely vibrational Franck−Condon factors. The extent of such effects will only become clear when detailed calculations of the photoionization dynamics of the NO_2 3pσ $^2\Sigma_u^+$ state are performed.

The small Franck−Condon factors for all but the vertical transition minimize the likelihood that vibrationally autoionizing states influence the branching fractions. In particular, any vibrationally autoionizing level would have at least one mode with $v_i \geq v_i^+ + 1$, as the three-photon energy in either ionization scheme lies above the diagonal threshold. The observation that the branching fractions are strongly diagonal also indicates that electronically autoionizing states are not accessed at the three-photon energy in this study.

Finally, Figure 7 shows the one ($\lambda_1 + \lambda_2 + \lambda_2$) photoelectron spectrum we obtained that exhibits anything like a vibrational progression, with peaks observed for $v_1 = 0-3$. However, even in this case, which was found for ionization via the 3pσ $^2\Sigma_u^+$

TABLE 4: Branching Fractions for Direct Ionization of Selected NO_2^+ X $^1\Sigma_g^+$ (v_1^+,v_2^+,v_3^+) States

prepared state	λ_1 ionization		λ_2 ionization	
3pσ $^2\Sigma_u^+$ v_1', v_2', v_3'	(v_1^+,v_2^+,v_3^+)	branching fraction for NO_2^+ $^1\Sigma_g^+$ (v_1^+,v_2^+,v_3^+)[a]	(v_1^+,v_2^+,v_3^+)	branching fraction for NO_2^+ $^1\Sigma_g^+$ (v_1^+, v_2^+, v_3^+)[a]
(000)	(000)	1.00	(000)	0.97
			(020)	0.03
(100)	(000)	0.04	(000)	0.01
	(100)	0.96	(100)	0.97
			(200)	0.02
			(300)	0.01
(010)	(000)	0.01	(010)	0.99
	(010)	0.99	(030)	0.01
(001)	(000)	0.01	(002)	0.01
	(100)	0.00	?	0.01
	(001)	0.99	(001)	0.99

[a] The branching fractions with values less than 0.05 have error bars of $\pm$0.01.

(100) level, the vertical transition accounts for ~98% of the signal, and a small difference in the potential surfaces of the Rydberg and ionic states could easily account for the progression in NO_2^+. It is interesting to note that, below the NO_2^+ $X^1\Sigma_g^+$ (100) threshold, vibrational autoionization of the (100) Rydberg series accessed from the $3p\sigma\ ^2\Sigma_u^+$ (100) state show the greatest rates for vibrational autoionization.[19,25,26] The interaction responsible for the coupling between these "discrete" Rydberg states and the $X^1\Sigma_g^+$ (000) also serves to couple the (100) and (000) continua above the $X^1\Sigma_g^+$ (100) threshold. Such continuum−continuum coupling could be at least partially responsible for the NO_2^+ progression in Figure 7, but again, this will only be determined when detailed calculations are performed.

V. Conclusions

A highly selective and very general method for preparing vibrationally state-selected NO_2^+ via two-color ionization via the $3p\sigma\ ^2\Sigma_u^+$ ($v_1v_2v_3$) Rydberg state has been developed. Specific approaches have been presented for producing NO_2^+ $X^1\Sigma_g^+$ in the (000), (001), (010), and (100) vibrational states. Photoionization of the $3p\sigma\ ^2\Sigma_u^+$ ($v_1v_2v_3$) by a single photon of either color resulted in ≥95% of the ions produced in the desired vibrational level. Experimental factors, such as the relative pulse energies of the two lasers, do not significantly affect the selectivity of these ionization schemes. The approach developed here should allow experiments on the vibrational mode dependence of the chemical reactivity of NO_2^+.

Acknowledgment. We thank Scott Anderson for helpful discussions about his work on the vibrational mode dependence of ion−molecule reactions. Patrice Bell's work at Argonne was supported through the Thesis Parts and Laboratory Graduate Programs of the ANL Division of Educational Programs. This work was supported by the U.S. Department of Energy, Office of Science, Office of Basic Energy Sciences, Division of Chemical Sciences, under Contract W-31-109-Eng-38. E.R.G. acknowledges support from the National Science Foundation under Grant CHE-0075833.

References and Notes

(1) Graul, S. T.; Squires, R. R. *Mass Spectrom. Rev.* **1988**, *7*, 263.
(2) Freiser, B. S. *Acc. Chem. Res.* **1994**, *27*, 353.
(3) Ervin, K. M. *Chem. Rev.* **2001**, *101*, 391.
(4) Luca, A.; Schlemmer, S.; Cermák, I.; Gerlich, D. *Rev. Sci. Instrum.* **2001**, *72*, 2900.
(5) Armentrout, P. B. *J. Am. Soc. Mass Spectrom.* **2002**, *13*, 419.
(6) (a) Baer, T. *Adv. Chem. Phys.* **1986**, *64*, 111. (b) Guyon, P. M.; Grover, T. R.; Baer, T. *Z. Phys. D: At., Mol. Clusters* **1986**, *4*, 89.
(7) (a) Jarvis, G. K.; Weitzel, K. M.; Malow, M.; Baer, T.; Song, Y.; Ng, C. Y. *Rev. Sci. Instrum.* **1999**, *70*, 3892. (b) Qian, X. M.; Zhang, T.; Chang, C.; Wang, P.; Ng, C. Y.; Chiu, Y. H.; Levandier, D. J.; Miller, J. S.; Dressler, R. A.; Baer, T.; Peterka, D. S. *Rev. Sci. Instrum.* **2003**, *74*, 4096.
(8) Softley, T. P.; Mackenzie, S. R.; Merkt, F.; Rolland, D. *Adv. Chem. Phys.* **1997**, *101*, 667.
(9) For early examples, see: Grant, E. R. In *Advances in Multiphoton Processes and Spectroscopy*; Lin, S. H., Ed.; World Scientific: Singapore, 1988 and references therein.
(10) Pratt, S. T. *J. Chem. Phys.* **2002**, *117*, 1055.
(11) Mark, S.; Glenewinkel-Meyer, T.; Gerlich, D. *Int. Rev. Phys. Chem.* **1996**, *15*, 283.
(12) (a) Anderson, S. L. *Acc. Chem. Res.* **1997**, *30*, 28. (b) Kim, H. T.; Liu, J.; Anderson, S. L. *J. Chem. Phys.* **2001**, *115*, 1274. (c) Liu, J.; Van Devener, B.; Anderson, S. L. *J. Chem. Phys.* **2002**, *117*, 8292. (d) Liu, J.; Van Devener, B.; Anderson, S. L. *J. Chem. Phys.* **2003**, *119*, 200.
(13) (a) Everest, M. A.; Poutsma, J. C.; Flad, J. E.; Zare, R. N. *J. Chem. Phys.* **1999**, *111*, 2507. (b) Flad, J. E.; Everest, M. A.; Poutsma, J. C.; Zare, R. N. *J. Chem. Phys.* **2001**, *124*, 124.
(14) Cheung, W. Y.; Chupka, W. A.; Colson, S. D.; Gauyacq, D.; Avouris, P.; Wynne, J. J. *J. Chem. Phys.* **1983**, *78*, 3625.
(15) (a) Lee, T. J.; Rice, J. E. *J. Phys. Chem.* **1992**, *96*, 650. (b) Grana, A. M.; Lee, T. J.; Head-Gordon, M. *J. Phys. Chem.* **1995**, *99*, 3493.
(16) Dignon, J. *Atmos. Environ.* **1992**, *26A*, 1157.
(17) McKeachie, J. R.; van der Veer, W. E.; Short, L. C.; Garnica, R. M.; Appel, M. F.; Benter, Th. *Analyst* **2001** *126*, 1221.
(18) Benit, J.; Bibring, J. P.; Rocard, F. *NATO ASI Ser., Ser. E* **1989**, *155*, 123.
(19) Campos, F. X.; Jiang, Y.; Grant, E. R. *J. Chem. Phys.***1990**, *93*, 2308.
(20) Campos, F. X.; Jiang, Y.; Grant, E. R. *J. Chem. Phys.***1992**, *96*, 7731.
(21) Bryant, G. P.; Jiang, Y.; Grant, E. R. *J. Chem. Phys.* **1992**, *96*, 4827.
(22) Bryant, G. P.; Jiang, Y.; Martin, M.; Grant, E. R. *J. Chem. Phys.* **1994**, *101*, 7199.
(23) Matsui, H.; Mayer, E. E.; Grant, E. R. *J. Mol. Spectrosc.* **1996**, *175*, 203.
(24) Matsui, H.; Behm, J. M.; Grant, E. R. *Int. J. Mass Spectrom. Ion Processes* **1996**, *159*, 37.
(25) Bell, P.; Aguirre, F.; Grant, E. R.; Pratt, S. T. *J. Chem. Phys.* **2003**, *119*, 10146.
(26) Bell, P.; Aguirre, F.; Grant, E. R.; Pratt, S. T. *J. Chem. Phys.*, in press.
(27) Kruit, P.; Read, F. H. *J. Phys. E: Sci. Instrum.* **1983**, *16*, 313.
(28) Glab, W. L.; Dehmer, P. M.; Dehmer, J. L. *J. Chem. Phys.* **1996**, *104*, 4937.
(29) Glab, W. L.; Glynn, P. T.; Dehmer, P. M.; Dehmer, J. L.; Wang, K.; McKoy, V. *J. Chem. Phys.* **1997**, *106*, 5779.
(30) Bunker, P. R.; Jensen, P. *Molecular Symmetry and Spectroscopy*; NRC Research Press: Ottawa, Canada, 1998.
(31) Brown, J. M.; Steimle, T. C.; Coles, M. E.; Curl, R. F., Jr. *J. Chem. Phys.* **1981**, *74*, 3668.
(32) Delon, A.; Dupre, P.; Jost, R. *J. Chem. Phys.* **1993**, *99*, 9482.
(33) Jost, R. *Int. J. Quantum Chem.* **1997**, *64*, 571.
(34) Guizard, S.; Shafizadeh, N.; Horani, M.; Gauyacq, D. *Chem. Phys.* **1991**, *156*, 509.
(35) Burgess, A.; Seaton, M. *Mon. Not. R. Astron. Soc.* **1960**, *120*, 121.